Electronic Supplementary Material (ESI) for Polymer Chemistry

Electronic Supplementary Information

Synthesis and characterization of highly porous borazine-linked polymers and their application to small gas storage

Karl T. Jackson, Mohammad G. Rabbani, Thomas E. Reich, and Hani M. El-Kaderi*

Department of Chemistry, Virginia Commonwealth University,

1001 W. Main St., Richmond, Virginia 23284

* To whom correspondence should be addressed. E-Mail: helkaderi@vcu.edu

Materials and Methods Table of Contents

Materials and Methods Section S1: Full synthetic procedures for the preparation of p-$C_6H_4(NH_2{\cdot}BH_3)_2$, $C(C_6H_4NH_2{\cdot}BH_3)_4$, BLP-1(H) and BLP-12(H).

General Synthetic Procedures: All starting materials and solvents, unless otherwise noted, were obtained from the Acros Organics Co. and used without further purification. *P*-phenylenediamine was purified by sublimation. Tetrahydrofuran (THF) and monoglyme were distilled over sodium and benzophenone and dichloromethane (DCM) was distilled over CaH_2. *Tetra*-(4-aminophenyl)methane was synthesized according to a published method.[1] The isolation and handling of all products were performed under an inert atmosphere of nitrogen using either glove box or Schlenk line techniques.

Synthesis of *p*-$C_6H_4(NH_2{\cdot}BH_3)_2$. A 100 ml Schlenk flask was charged with *p*-phenylenediamine (200 mg, 1.85 mmol) and 100 ml of anhydrous DCM. The solution was cooled to -78 ºC in an acetone/dry ice bath and treated with borane-dimethylsulfide (1.05 ml, 11.1 mmol, Aldrich) drop-wise under a flow of nitrogen. The clear solution was allowed to warm to room temperature while stirring overnight. On the following day, the white solid material is filtered and washed with DCM (3x15ml).^{1}H NMR: (300 MHz, d_6-DMSO) δ 7.39 (s, 4H), 7.11 (s, 4H), 1.51 (s, br, 6H).^{13}C NMR (75 MHz, d_6-DMSO) δ 123.12, 141.30.

Further characterization by Mass Spectrometry and elemental analysis were unsuccessful due to the instability of the amine-borane adduct in the absence of solvents and due to polymerization upon heating under elemental analysis testing conditions.

Synthesis of BLP-1(H). A Pyrex tube was charged with *p*-$C_6H_4(NH_2{\cdot}BH_3)_2$ (35 mg, 0.26 mmol) and 2 ml of glyme. The tube was flash frozen at 77 K, evacuated and flame sealed. The reaction mixture was heated in a programmable oven at 0.1 ºC/min to 120 ºC for 24 h to afford a fluffy white polymer which was isolated by filtration over a medium glass frit and washed with

anhydrous THF (3 x 15 ml). Anal. Calcd.for ($C_9H_9B_3N_3$): C, 56.4%; H, 4.7%; N, 21.9%. Found: C, 55.85%; H, 5.13%; N, 18.23%.*

Synthesis of $C(C_6H_4NH_2{\cdot}BH_3)_4$. A 100 ml Schlenk flask was charged with *tetra*-(4-aminophenyl)methane (100 mg, 0.26 mmol) and 100 ml of anhydrous DCM. The suspension was cooled to 0 ºC in an ice bath under a flow of nitrogen and treated with borane-dimethylsulfide (0.30 ml, 3.16 mmol) drop-wise. The clear solution was allowed to warm to room temperature while stirring overnight. On the following day, the white solid material is filtered and washed with DCM (3 x 15ml). ^{1}H NMR (300 MHz, d_6 DMSO) δ 7.47 (s, br, 8H), 7.14-7.17 (m, 16H), 1.59 (s, br, 12H). ^{13}C NMR (75 MHz, d_6-DMSO) δ 63.81, 122.35, 131.22, 141.69, 144.23.

Further characterization by Mass Spectrometry and elemental analysis were unsuccessful due to the instability of the amine-borane adduct in the absence of solvents and due polymerization upon heating under elemental analysis testing conditions.

Synthesis of BLP-12(H). A Pyrex tube was charged with 30 mg of $C(C_6H_4NH_2{\cdot}BH_3)_4$ (35 mg, 0.08 mmol) was dissolved in 2 ml of glyme. The tube was flash frozen at 77 K, evacuated and flame sealed. The reaction mixture was heated in a programmable oven at 0.1 ºC/min to 120ºC for 24 h to afford a fluffy white polymer which was isolated by filtration over a medium glass frit and washed with anhydrous THF (3 x 15 ml).Anal. Calcd. for ($C_{75}H_{60}B_{12}N_{12}$): C, 71.54%; H, 4.80%; N, 13.35%. Found: C, 60.93%; H, 4.94%; N, 9.87%.*

**Organoboron compounds typically give lowered carbon values in elemental microanalysis due to the formation of non-combustible boron carbide byproducts.*[2]

Activation of BLPs for gas adsorption measurements. Inside a glove-box, about 150 mg of as-prepared sample of BLP was loaded into an Autosorb cell then heated to 120 °C under dynamic vacuum (1.0 x 10^{-5} torr) for 16 h. The sample was back-filled with nitrogen to exclude adsorption of moisture prior to N_2 adsorption measurements.

Materials and Methods Section S2: FT-IR Spectroscopy of Starting Materials, BLP-1(H) and BLP-12(H).

FT-IR data was used to verify that the products were being produced. By observing the loss of certain stretches expected for dehydrocoupling reactions combined with the appearance of borazine-characteristic peaks, the formation of the expected products can be confirmed. FT-IR spectra of starting materials, BLP-1(H) and BLP-12(H) were obtained as KBr pellets using Nicolet - Nexus 670 spectrometer. The bands at 3300-3500 cm^{-1} that correspond to the N-H stretching of amine/amine-borane adducts are significantly reduced after polymerization, however, the remaining weak signals are due to N-H stretches from unreacted $–NH_2$ on the surface of the polymers' particles and incompletely reacted groups at defects in the material. The aromatic C-H stretching was observed around 2800-3100 cm^{-1}. Borane B-H peaks in adducts were observed at approximately 2400 cm^{-1} while a slight shift to about 2550 cm^{-1} occurs after the formation of the borazine ring during polymerization. The N-H band stretch of the amine is greatly reduced indicating a release of the amine hydrogen atoms from the starting material. The strong stretch appearing at 1400 cm^{-1} also supports the formation of the B-N bonds of the borazine ring.

Figure S1: FT-IR spectrum of *p*-phenylenediamine.

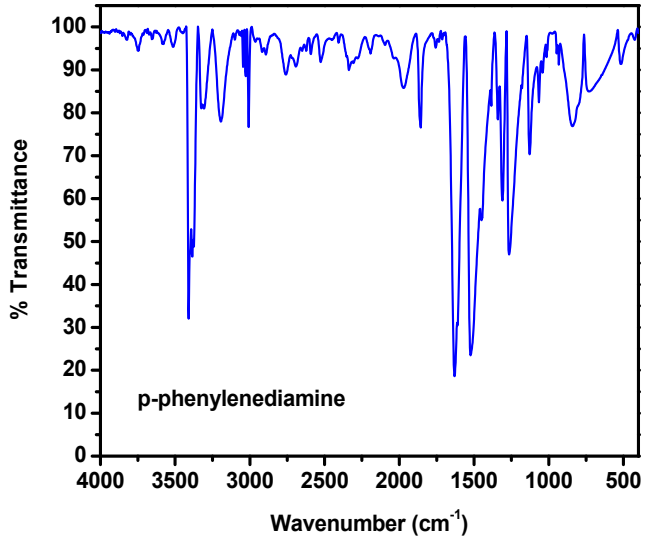

Figure S2: FT-IR spectrum of *Tetra*-(4-aminophenyl)methane.

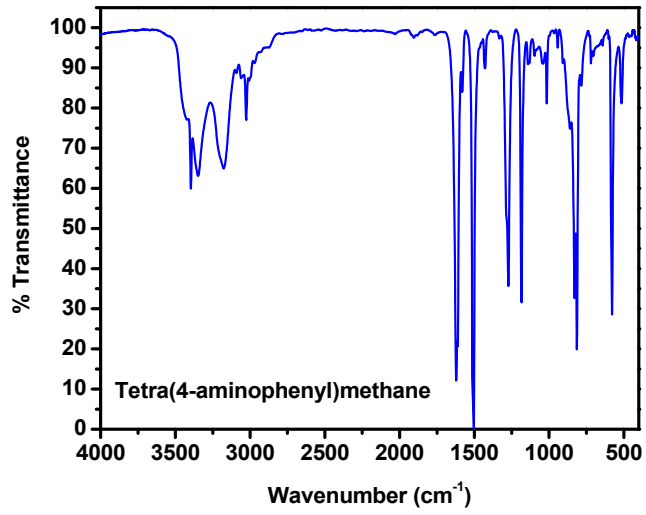

Figure S3: FT-IR spectrum of *p*-$C_6H_4(NH_2{\cdot}BH_3)_2$.

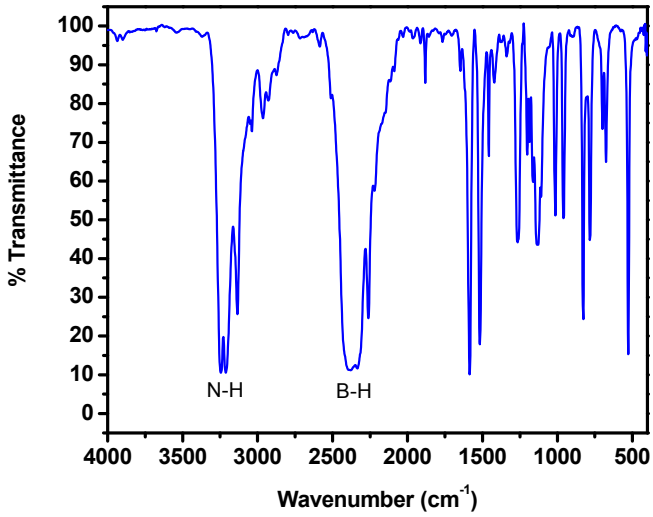

Figure S4: FT-IR spectrum of $C(C_6H_4NH_2{\cdot}BH_3)_4$.

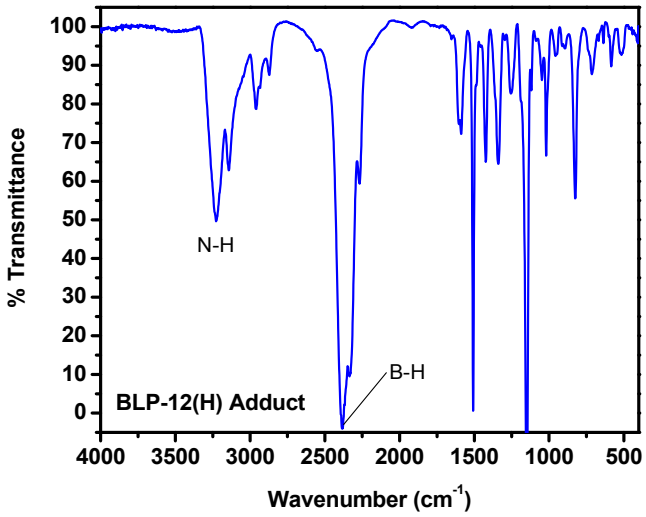

Figure S5: FT-IR spectrum of BLP-1(H).

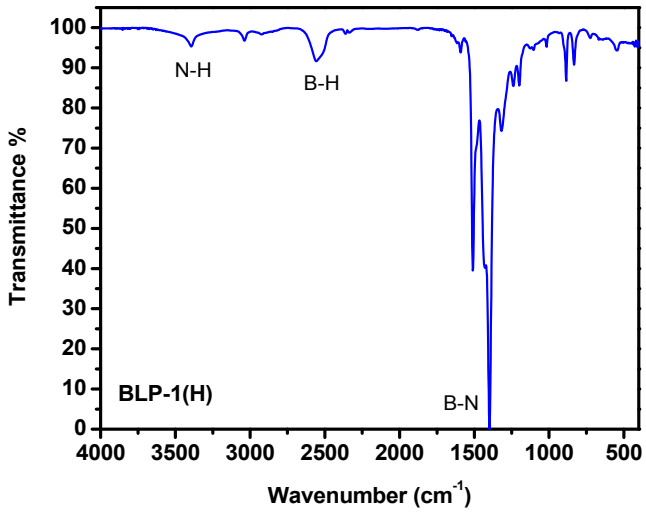

Figure S6: FT-IR spectrum of BLP-12(H).

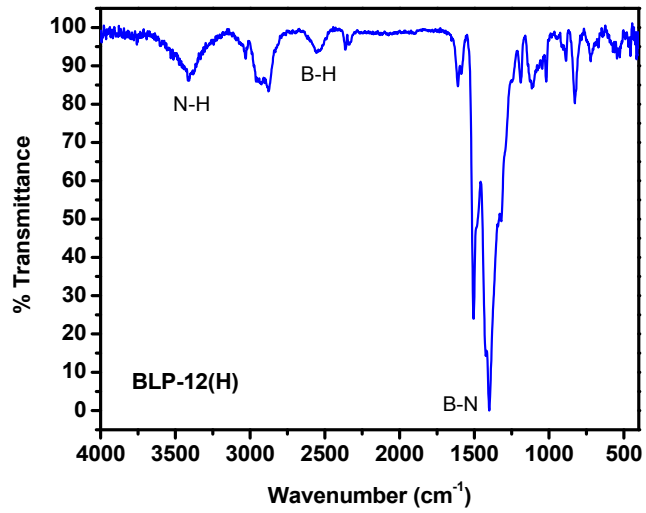

Figure S7: FT-IR spectrum of BLP-1(H).

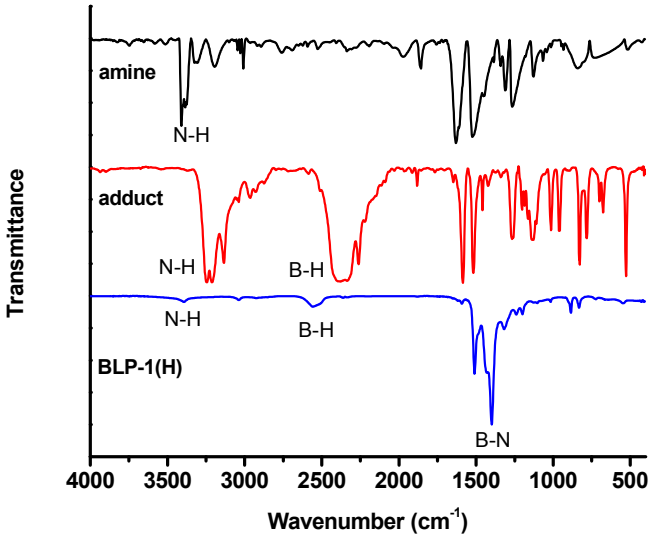

Figure S8: FT-IR spectrum of BLP-12(H).

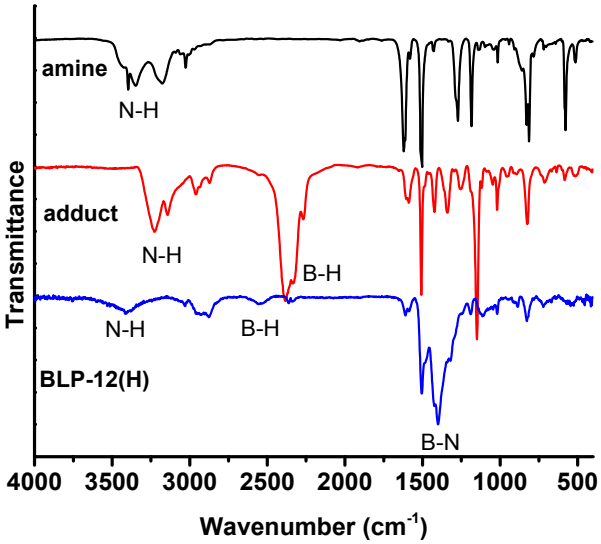

Materials and Methods Section S3: Solid-State ^{11}B and ^{13}C Cross-Polarization Magic Angle Spinning (CPMAS) Nuclear Magnetic Resonance

^{11}B MAS NMR data were collected with a 45 degree ^{11}B pulse length and a recycle delay of two seconds. High-power H-1 decoupling was employed during acquisition only. Samples were spun at the magic angle at about 7 kHz. Chemical shifts are referenced to external neat boron trifluoroetherate. Solid-state NMR spectra were recorded at ambient temperature on a 360-1 instrument by Spectral Data Services, Inc., Champaign, IL. *Asterisks represent spinning side bands.*

Figure S9: Solid state ^{13}C NMR for BLP-1(H)

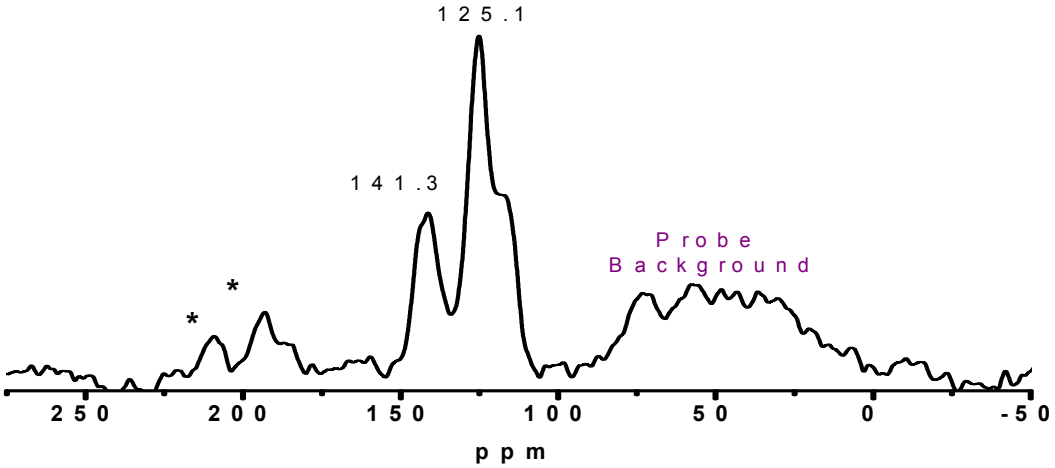

Figure S10: Solid state ^{11}B NMR for BLP-1(H)

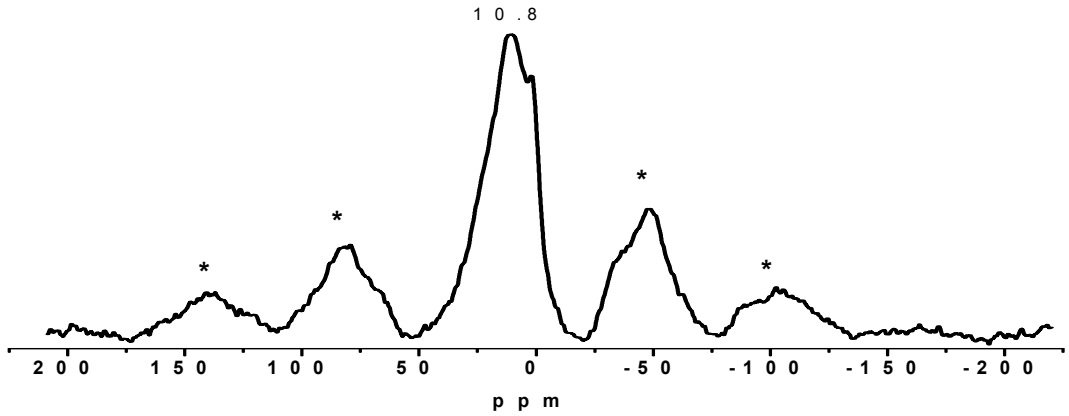

Figure S11: Solid state ^{13}C NMR for BLP-12(H)

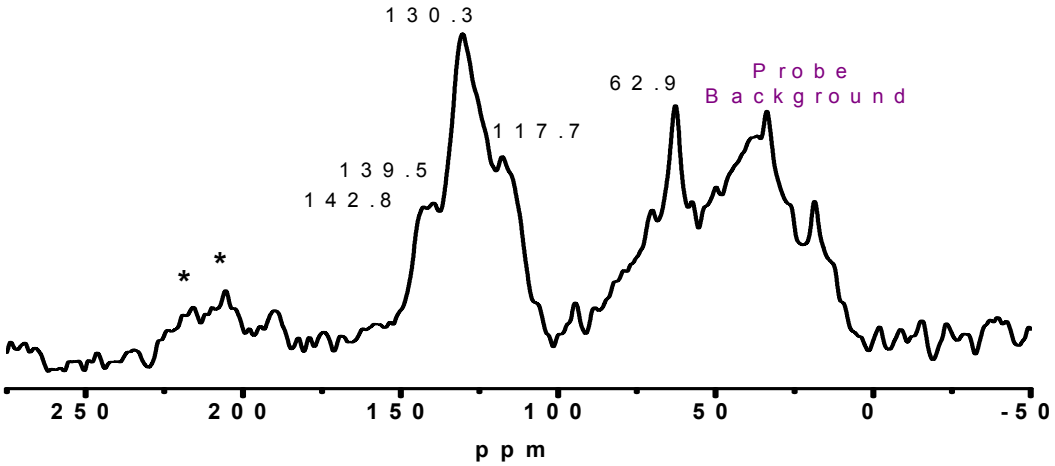

Figure S12: Solid state ^{11}B NMR for BLP-12(H).

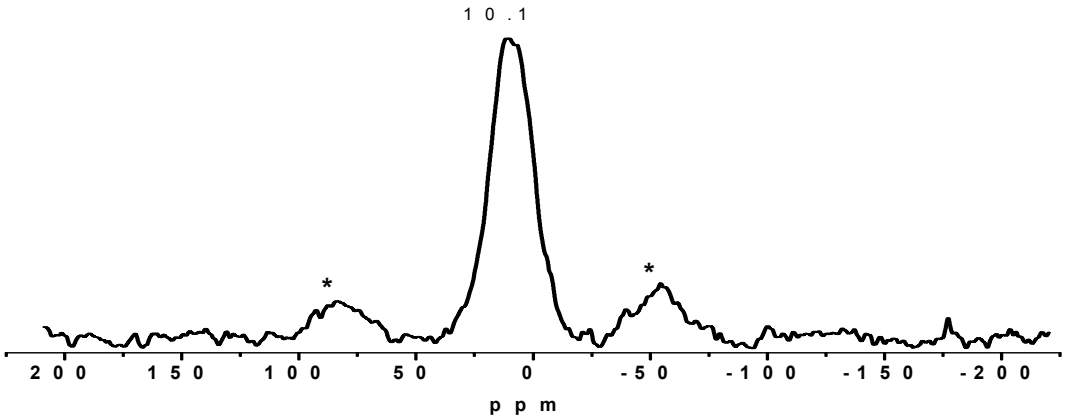

Materials and Methods Section S4: Scanning Electron Microscopy Imaging (SEM) for BLP-1(H) and BLP-12(H).

In order to determine the purity of products, SEM was used to scan for the morphology present in the sample. A sample of the BLP material was subjected to scrutiny under the SEM microscope. Only one type of morphology was found to exist, confirming the purity of the material produced. Sample was prepared by dispersing the material onto a sticky carbon surface attached to a flat aluminum sample holder. The sample was then gold coated using an EMS (Electron Microscopy Sciences) 550x Sputter Coater at $1x10^{-1}$ mbar of pressure in a nitrogen atmosphere for 120 seconds while maintaining 20 mA of current. Samples were analyzed on a Zeiss EVO XVP Scanning Electron Microscope using the SEI detector with accelerating voltages ranging from 10 kV to 20 kV.

Figure S13: SEM image of BLP-1(H) revealing a spherical morphology.

a)

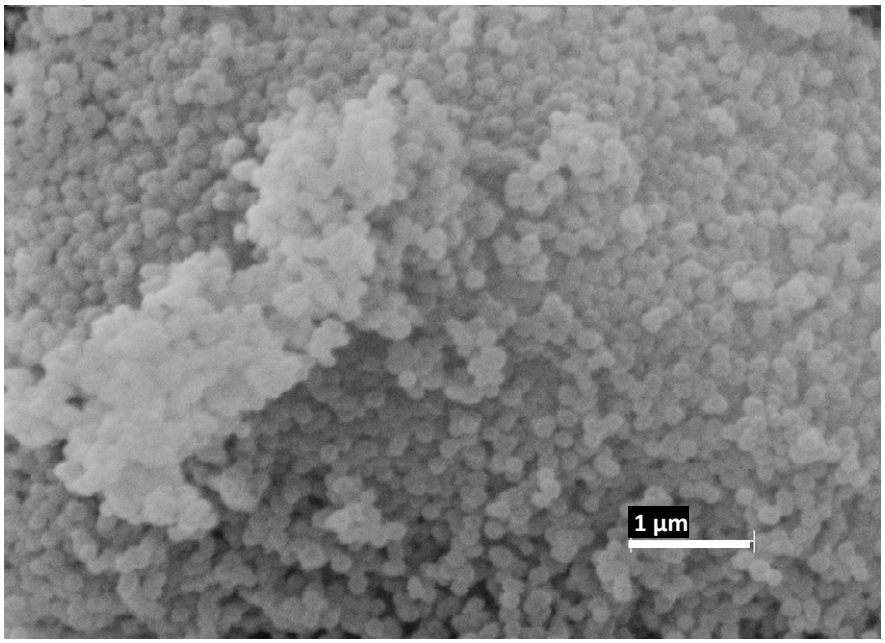

b)

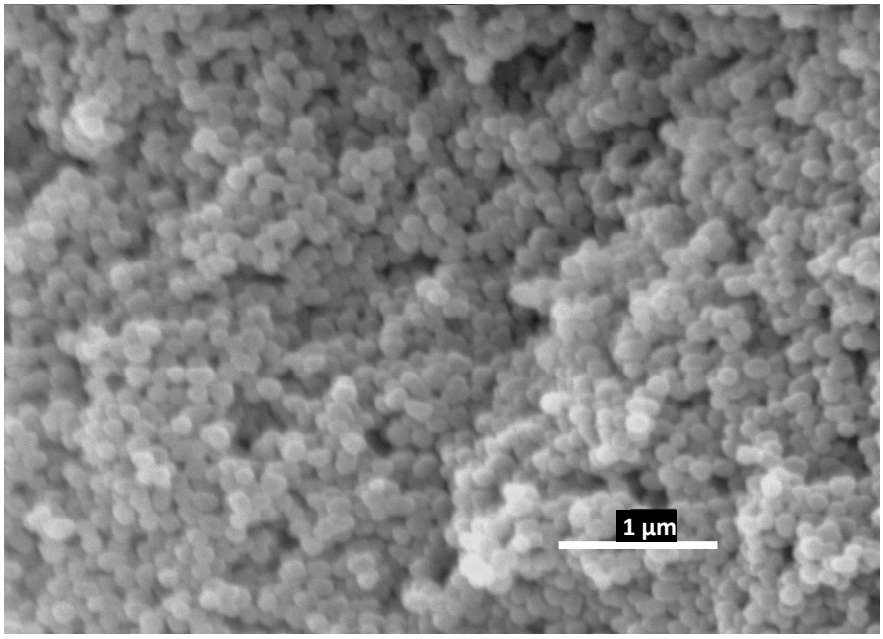

Figure S14: SEM image of BLP-12(H) revealing a platelet morphology.

a)

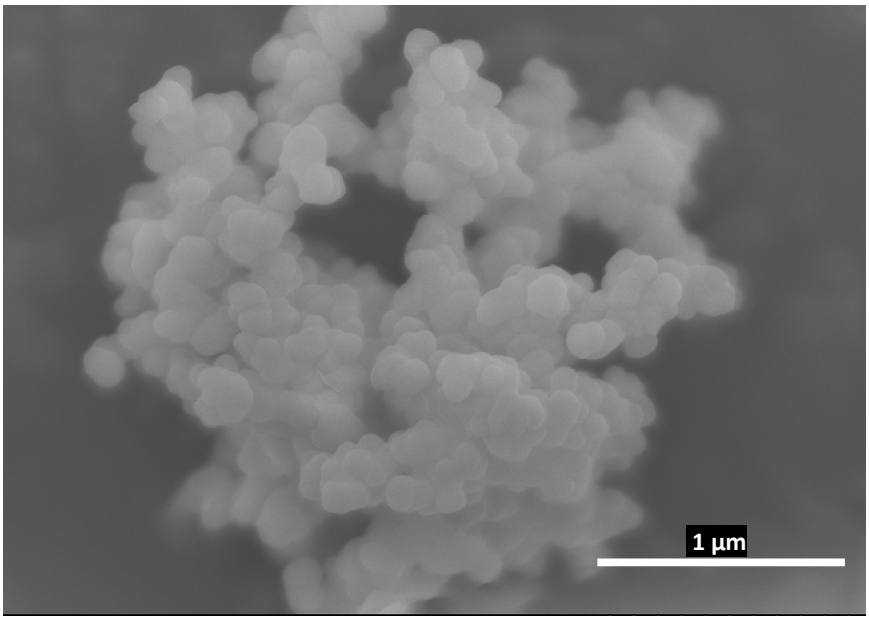

b)

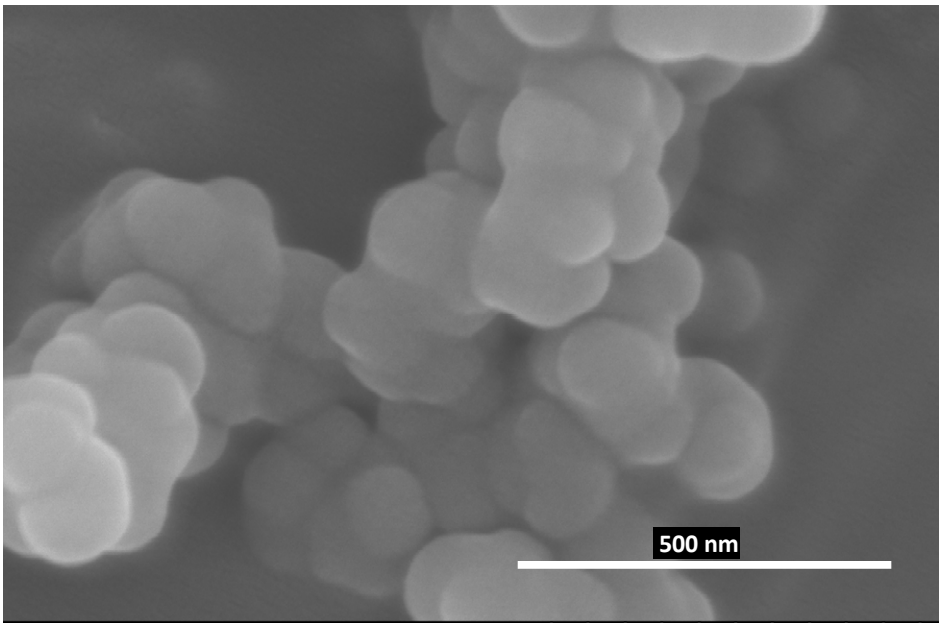

Materials and Methods Section S5: Thermogravimetric Analysis.

BLP-1(H) and BLP-12(H) were analyzed by TGA to determine the thermal stability of the material produced as well as confirm that all guests have been removed. Samples were run on a TA Instruments Q-5000 series thermal gravimetric analyzer with samples held in platinum pans under an atmosphere of nitrogen.

Figure S15: TGA trace for an unactivated sample of BLP-1(H).

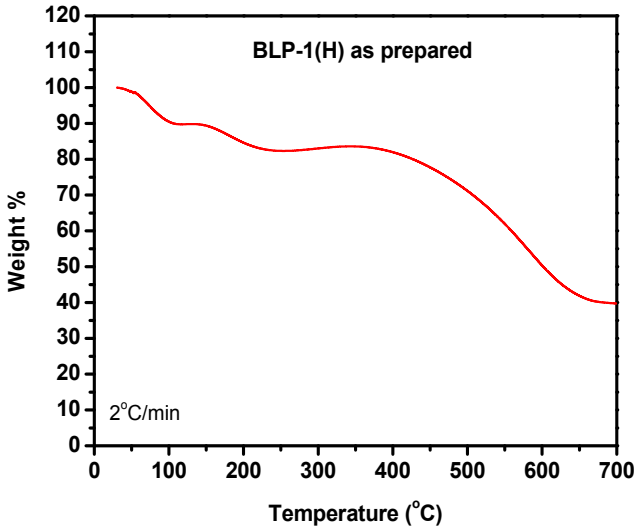

Figure S16: TGA trace for an unactivated sample of BLP-12(H).

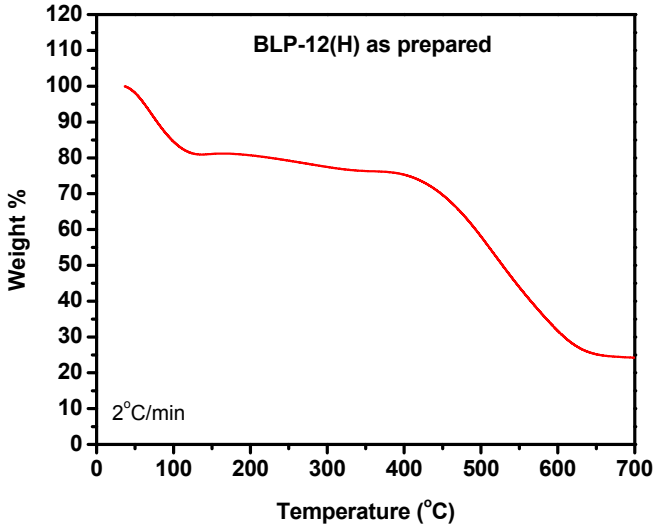

Materials and Methods Section S6: Low Pressure (0 – 760 mTorr) Nitrogen, Hydrogen, Methane and Carbon Dioxide Adsorption Measurements for BLP-1(H) and BLP-12(H).

Nitrogen experiments were run using a Quantachrome Autosorb 1-C analyzer at 77 K. Pore Size Distributions (PSDs) were calculated using Non-Local Density Functional Theory (NLDFT) on the adsorption branch with a spherical/cylindrical pore model. Hydrogen sorption experiments were run on the same Quantachrome Autosorb 1-C analyzer at both 77 K and 87 K. Methane and carbon dioxide experiments were run at 273 K and 293 K each. Ultrahigh purity helium (99.999%) was used to calibrate the free volume in the sample cell before each measurement. For H_2 uptake measurement, hydrogen with purity of 99.999% was used. CO_2 (99.9%) and CH_4 (99.999%) were obtained from Airgas Inc. (Radnor, PA).

Using the data taken at 77 K and 87 K, the isosteric heat of adsorption for each polymer was calculated according to previous reports[3] by solving the virial-type expression:

$$\ln P = \ln N + (1/T)\sum_{i=0}^{m} a_i N^i + \sum_{i=0}^{n} b_i N^i$$

where P is pressure in torr, T is temperature in Kelvin, and N is the mmol of gas adsorbed per gram of sample. The values for *m* and *n* were varied such that $m \geq n$ and resulted in the best fit as determined by the sum of the squares of the errors. The values for a_0, a_1,…a_m were used in the calculation for the isosteric heat of adsorption, Q_{st}:

$$Q_{st} = -R\sum_{i=0}^{m} a_i N^i$$

The calculated values were plotted as they relate to surface coverage, and the isosteric heat of adsorption values at the point of zero-coverage were highlighted in the text.

Figure S17: N_2 adsorption isotherm for BLP-1(H) (blue) and BLP-12(H) (red) measured at 77 K. The filled squares are adsorption points and the empty squares are desorption points.

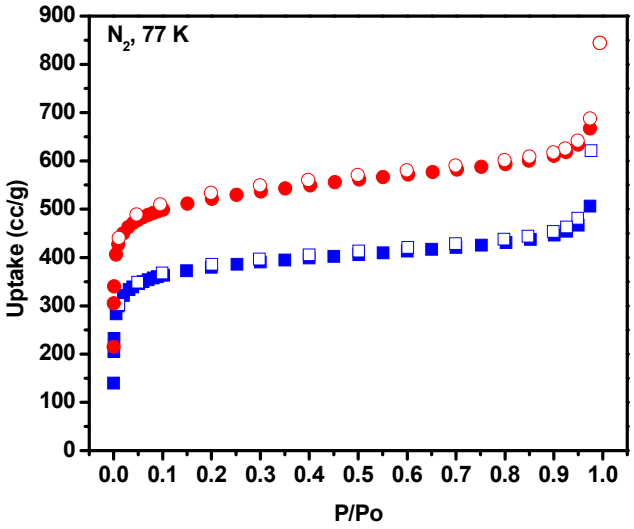

Pore Size Distributions (PSDs) were calculated using Non-Local Density Functional Theory (NLDFT) on the adsorption branch with a cylindrical/sphere pore model on the nitrogen experiments combined with data taken from carbon dioxide sorption experiments performed at 273 K as has been reported previously.[2]

Figure S18: NLDFT Pore Size Distribution for BLP-1(H)

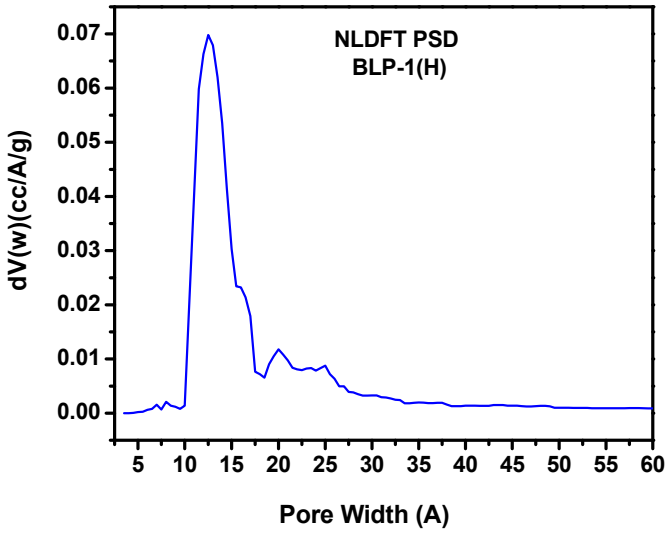

Figure S19: NLDFT Pore Size Distribution for BLP-12(H)

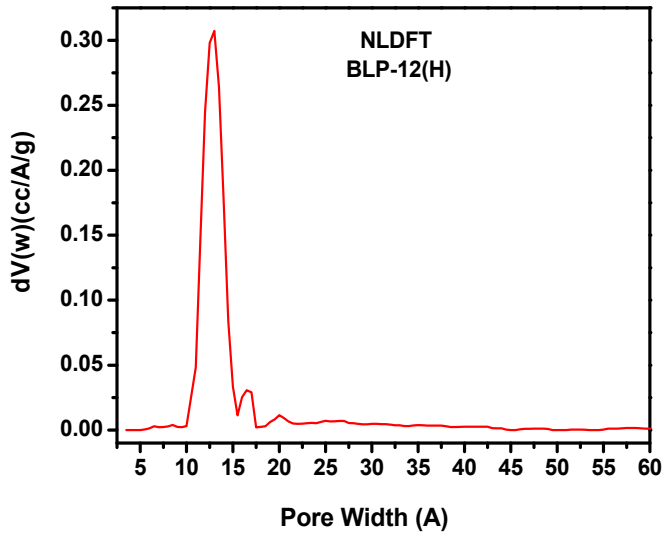

Figure S20: Experimental N_2 adsorption isotherm for BLP-1(H) measured at 77 K is shown as filled squares. The calculated NLDFT isotherm is overlaid as open squares. Note that a fitting error of < 1 % indicates the validity of using this method for assessing the porosity of BLP-1(H). The fitting error is indicated.

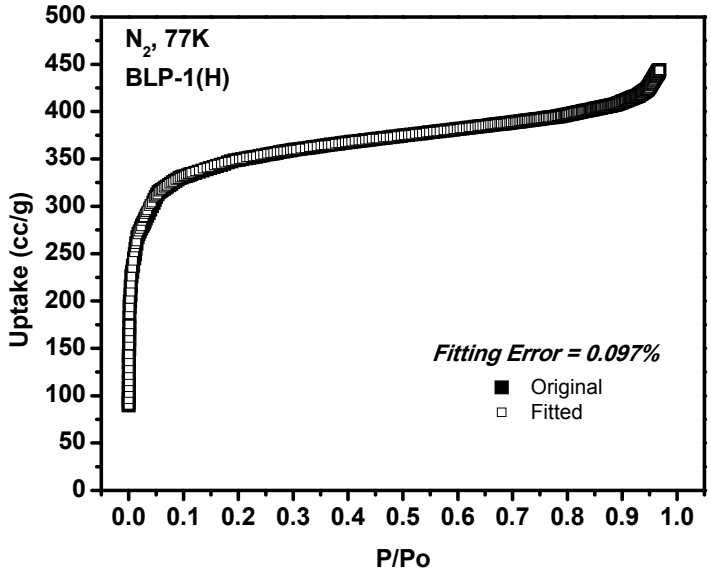

Figure S21: Experimental N_2 adsorption vs. calculated NLDFT isotherm for BLP-12(H)

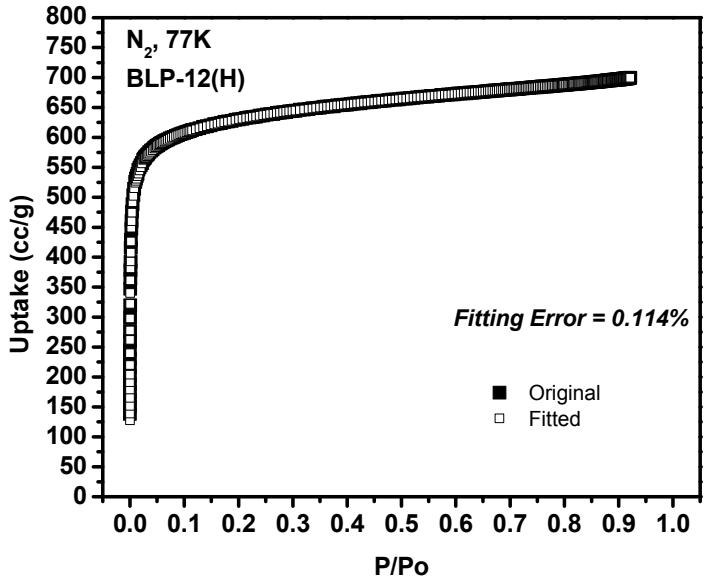

Figure S22: BET plot for BLP-1(H) calculated from the N_2 adsorption isotherm at 77 K. The model was applied from P/P_o= 0.05-0.15. The correlation factor is indicated.

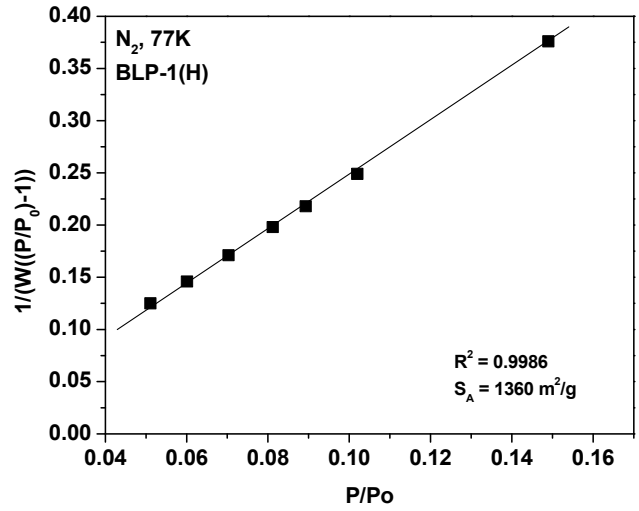

Figure S23: BET plot for BLP-12(H)

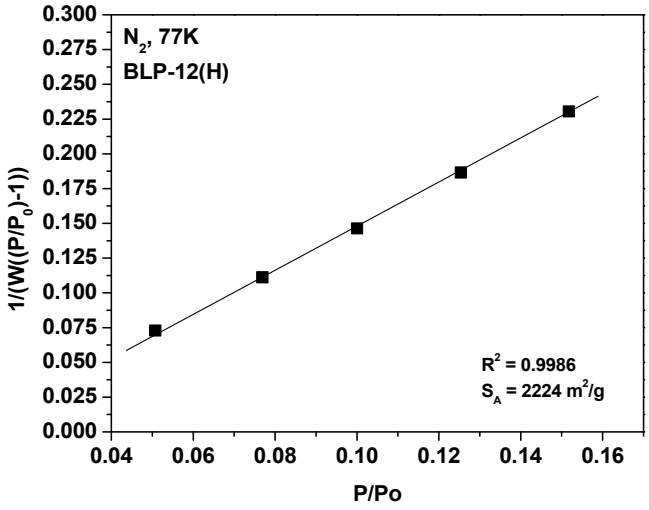

Figure S24: Langmuir plot for BLP-1(H) calculated from the N_2 adsorption isotherm at 77 K. The model was applied from P/P_o= 0.05-0.30. The correlation factor is indicated.

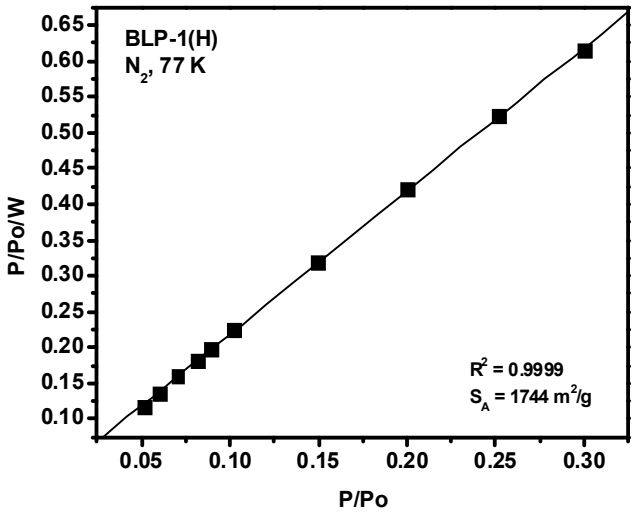

Figure S25: Langmuir plot for BLP-12(H)

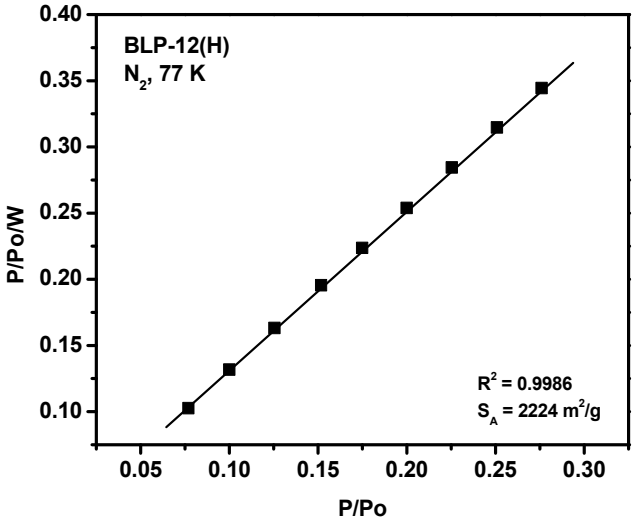

Table S1: Hydrogen Storage Properties of BLP-1(H) and BLP-12(H)

	H_2				
	cc/g	mmol/g	mg/g	wt%	Q_{st} (kJ/mol)
BLP-1(H)	148	6.66	13.3	1.33	6.8
BLP-12(H)	214	9.64	19.3	1.93	5.9

Table S2: Carbon Dioxide Storage Properties of BLP-1(H) and BLP-12(H)

	CO_2				
	cc/g	mmol/g	mg/g	wt%	Q_{st} (kJ/mol)
BLP-1(H)	37.4	1.68	73.9	7.39	25.3
BLP-12(H)	64.8	2.91	128	12.8	25.2

Table S3: Methane Storage Properties of BLP-1(H) and BLP-12(H)

	CH_4				
	cc/g	mmol/g	mg/g	wt%	Q_{st} (kJ/mol)
BLP-1(H)	10.8	0.48	7.74	0.77	23.9
BLP-12(H)	17.4	0.78	12.5	1.25	17.0

Figure S26: H_2 adsorption isotherm for BLP-1(H) measured at 77 K (red circles) and 87K (blue diamonds). The filled shapes are adsorption points and the empty shapes are desorption points.

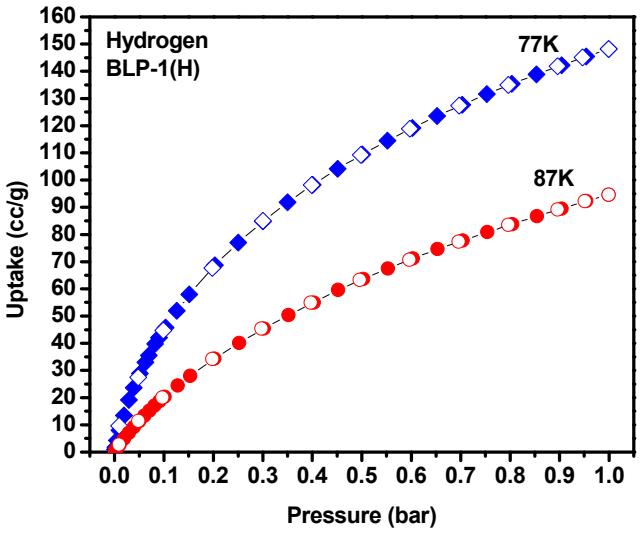

Figure S27: Hydrogen isosteric heat of adsorption (Q_{st}) for BLP-1(H).

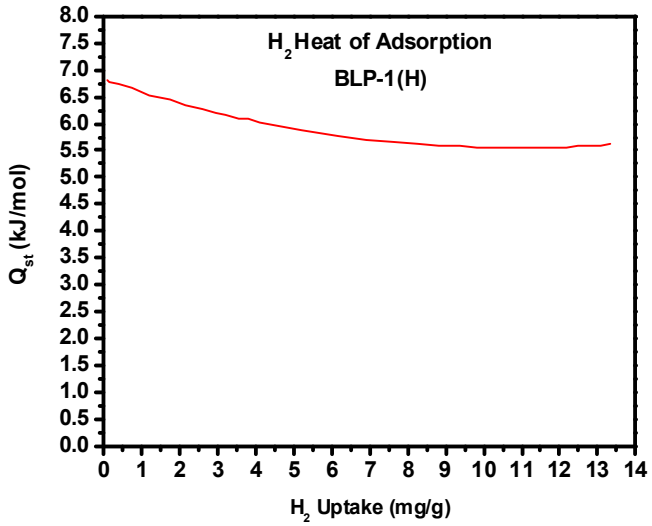

Figure S28: H_2 adsorption isotherm for BLP-12(H) measured at 77 K (red circles) and 87K (blue circles). The filled shapes are adsorption points and the empty shapes are desorption points.

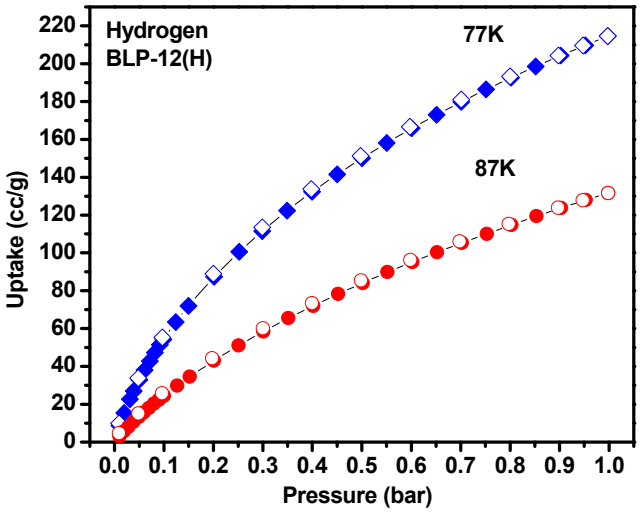

Figure S29: Hydrogen isosteric heat of adsorption (Q_{st}) for BLP-12(H).

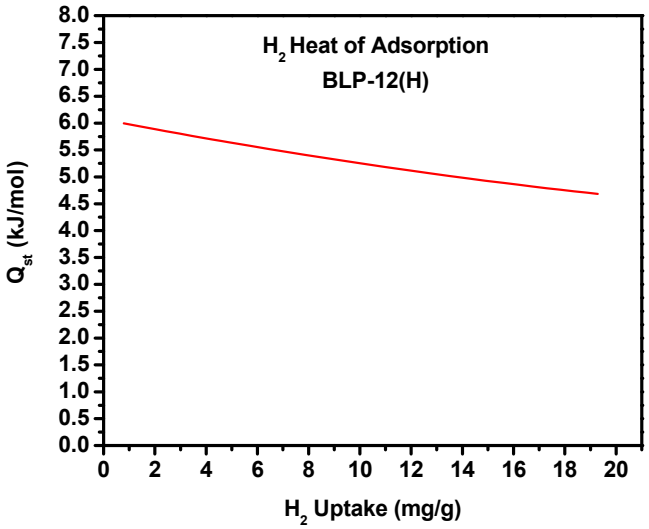

Figure S30: Methane adsorption isotherm for BLP-1(H) measured at 273K (red squares) and 293 K (blue circles). The filled shapes are adsorption points and the empty shapes are desorption points.

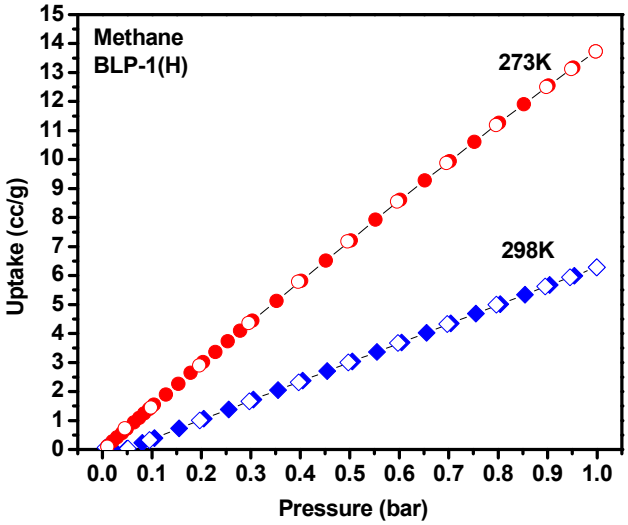

Figure S31: Methane isosteric heat of adsorption (Q_{st}) for BLP-1(H).

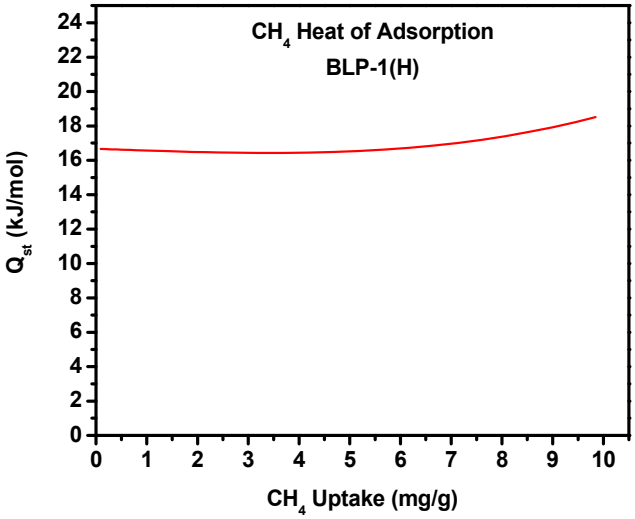

Figure S32: Methane adsorption isotherm for BLP-12(H)

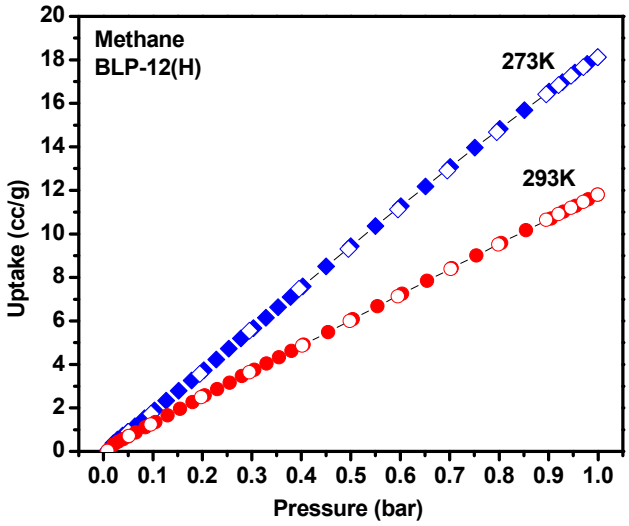

Figure S33: Methane isosteric heat of adsorption (Q_{st}) for BLP-12(H).

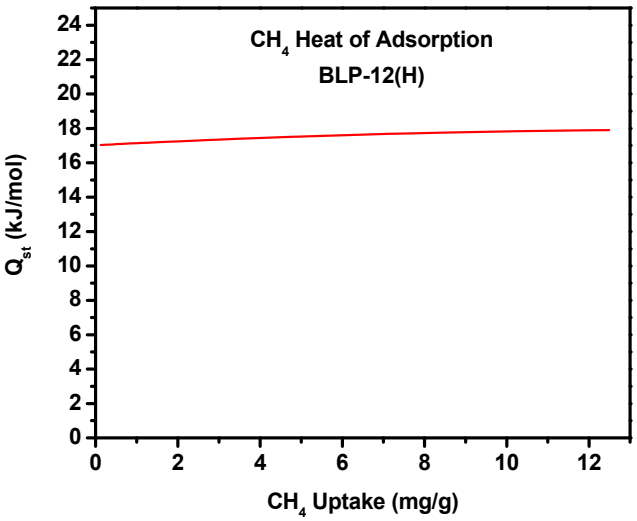

Figure S34: Carbon dioxide adsorption isotherm for BLP-1(H).

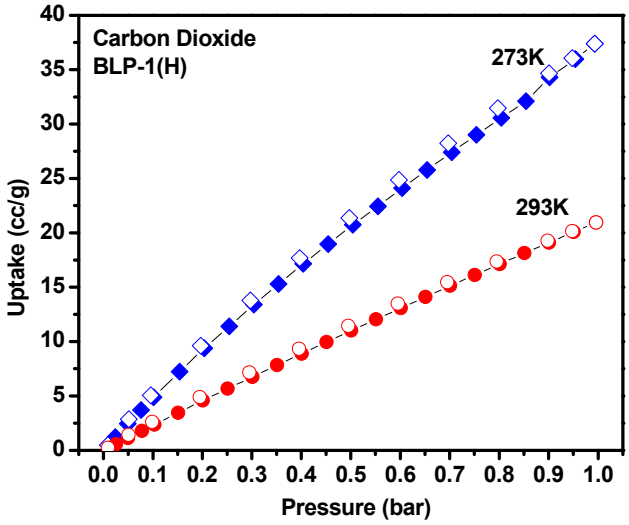

Figure S35: Carbon dioxide isosteric heat of adsorption (Q_{st}) for BLP-1(H).

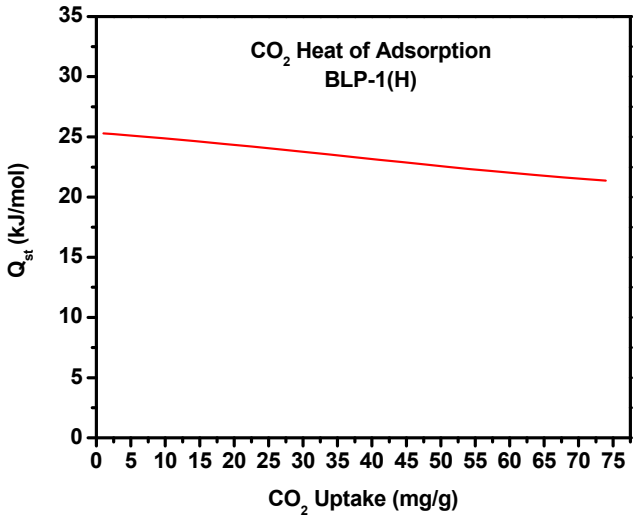

Figure S36: Carbon dioxide adsorption isotherm for BLP-12(H)

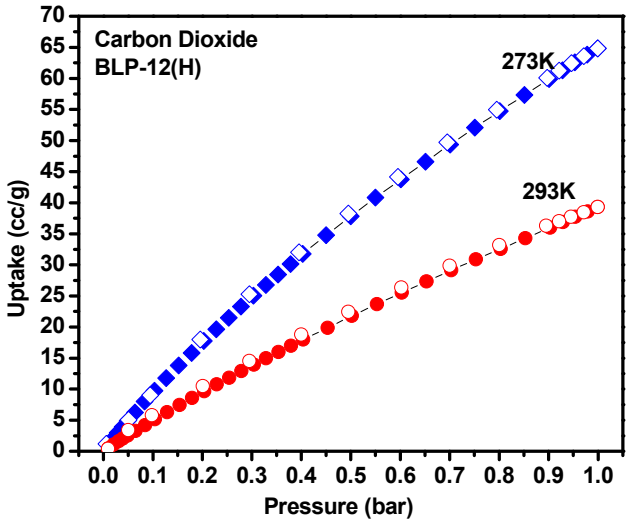

Figure S37: Carbon dioxide isosteric heat of adsorption (Q_{st}) for BLP-12(H).

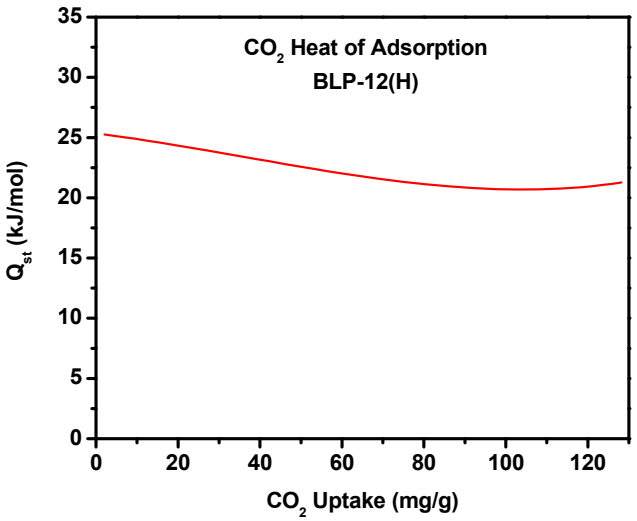

References

1. P. Ganesan, X. Yang, J. Loos, T. J. Savenije, R. D. Abellon, H. Zuilhof, E. J. R. Sudhölter, *J. Am. Chem. Soc.* 2005, **127**, 14530.

2. Cote, A. P.; Benin, A. I.; Ockwig, N. W.; O'Keeffe, M.; Matzger, A. J.; Yaghi, O. M. *Science* 2005, **310**, 1166.

3. Jagiello, J.; Bandosz, T. J.; Putyera, K.; Schwarz, J. A. *J. Chem. Eng. Data* 1995, **40**, 1288.